Geophys. J. R. astr. Soc. (1985) **83**, 519–539

Upper crustal shear velocity models from higher mode Rayleigh wave dispersion in Scotland

Colin D. MacBeth* and Paul W. Burton *Natural Environment Research Council, British Geological Survey, Murchison House, West Mains Road, Edinburgh EH9 3LA*

Accepted 1985 April 18. Received 1985 April 15; in original form 1984 August 21

Summary. Group velocities for first and second higher mode Rayleigh waves, in the frequency range 0.8–4.8 Hz, generated from a local earthquake of magnitude 3.7 M_L in western Scotland, are measured at stations along the 1974 LISPB line. These provide detailed information about the crustal structure west of the line. The data divide the region into seven apparently homogeneous provinces. Averaged higher mode velocity dispersion curves for each province are analysed simultaneously using a linearized inversion technique, yielding regionalized shear velocity profiles down to a depth of 17 km into the upper crust. Shear wave velocity is between 3.0 and 3.4 km s^{-1} in the upper 2 km, with a slow increase to around 3.8 km s^{-1}. *P*-wave models computed using these results agree with profiles from the LISPB and LUST refraction experiments.

Key words: crustal structure, Rayleigh waves, Scotland, seismology

1 Introduction

Most of the available crustal velocity models for Britain have been estimated from refraction experiments such as LISPB (Bamford *et al.* 1976, 1977, 1978) and LUST (Hall 1978). At short epicentral distances, these studies concentrate on evaluating compressional wave velocity structures since the *S*-wave arrivals are usually masked by *P*-wave coda. Consequently, important information on the velocity ratio of the two types of body wave (which is indicative of lithology) is usually excluded. The seismic refraction studies are also restricted by the classical 'hidden layer' problem concerning low velocity zones. Higher mode surface waves provide an alternative means of measuring the distribution of shear velocity with depth in these cases.

There have been very few studies of seismic surface waves propagating in Scotland. Evans (1981) carried out the first extensive analysis of fundamental mode Rayleigh waves using data generated by the small explosions of the LISPB experiment. The seismograms proved to be of sufficient quality to enable accurate measurements of frequency-dependent group

* Also at: Department of Geophysics, University of Edinburgh, Mayfield Road, Edinburgh EH9 3JZ.

velocity, inter-station phase velocity and the Rayleigh wave specific attenuation factor. These were analysed according to the surface geological expression, providing high resolution velocity and attenuation data for the near surface crustal structure of Scotland. However, these data were limited to depths of 2 km, as the fundamental mode energy could only resolve to 0.4 λ_m, where λ_m is the maximum Rayleigh wavelength (Knopoff & Schlue 1972). Inversions involving higher modes, which sample much larger crustal depths, overcome this problem (Bloch, Hales & Landisman 1969). Further, simultaneous inversion of dispersion data from many modes increases the accuracy and resolution that can be attained (Braille & Keller 1975). This type of data enables depths 10 times greater than the source depth to be discerned (Nolet 1977). Unfortunately, higher mode data are difficult to obtain at regional distances unless sophisticated techniques such as the stacking method of Nolet (1975) are utilized.

This paper presents higher mode group velocity data from a small earthquake in the Kintail region of western Scotland recorded locally on short-period seismometers. The recordings contain well separated first and second higher mode Rayleigh waves. Velocity structures are obtained by simultaneously inverting first and second higher mode group velocities in the frequency range 0.8–4.8 Hz. The results augment the information obtained from the shallow profiles of Evans (1981) and complement the *P*-wave cross-sections of Bamford *et al.* (1978).

2 Rayleigh wave data and dispersion analysis

2.1 THE DATA

In 1974 August a swarm of earthquakes with a maximum surface wave magnitude of 4.6 M_L occurred in the Kintail region of NW Scotland. One earthquake in this series, hereafter referred to as KEQ (M_L = 3.7), was recorded on the 60 stations comprising the LISPB ALPHA and BETA lines, giving a range of epicentral distances from 79 to 300 km and an azimuthal range from 15° to 146°. The relative position of KEQ with respect to the array is shown in Fig. 1. Kaminski *et al.* (1976) determined the hypocentre of this earthquake together with a plane layered velocity model for the region by fitting to first and second *P*-wave arrival data. Assumpção (1981) relocated the earthquake with *P* and *S* arrivals using the LISPB *P*-wave velocity model of Bamford *et al.* (1978) and the shear velocity model of Assumpção & Bamford (1978). For this, the structure at the epicentre was assumed similar to that of the LISPB profile north of the Loch Tay Fault (Fig. 1). The focal solution was given by Assumpção (1981) as:

1974 August 6, origin time 18 hr 17 min 36.93 ± 0.2 s (GMT),
latitude 57.227°N ± 2 km,
longitude 5.338°W ± 3km,
depth 10.6 ± 2 km,

allowing for uncertainties in the crustal structure. The depth was over 3 km shallower than that estimated by Kaminski *et al.* (1976). Well correlated signal waveforms implied that the Kintail events had the same focal mechanism. A composite focal plane solution was therefore obtained for these events using polarities of the first *P*-wave arrivals. The predominant rupture mechanism was left lateral strike-slip with a strike of 52°E of N and a dip of 74°S. The Strathconan fault system appeared to be associated with the swarm.

The recordings of KEQ, available to the authors at a sampling rate of 100 sps, are decimated to 25 sps (Dziewonski & Hales 1972). Figs 2–4 show the digitized Rayleigh waves

for the complete set of vertical component recordings of KEQ, azimuth and station code for each being marked. Dotted lines indicating velocities of 3.5, 3.0 and 2.5 km s^{-1} are shown for guidance. Inspection of the seismograms reveals three distinct portions corresponding to strong first and second higher mode arrivals (these are identified in the figure for stations A34, A36 and B02), and a very weak apparent fundamental mode arrival. The identity of

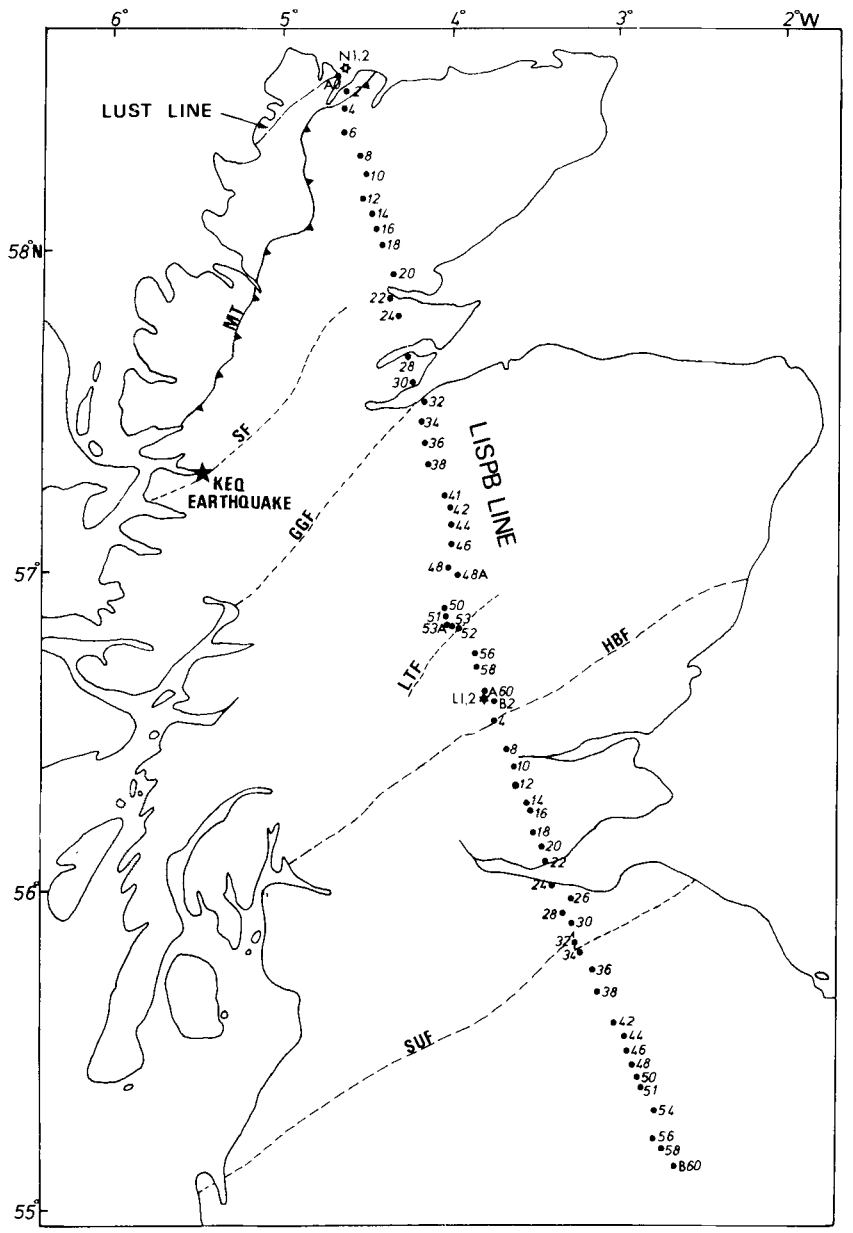

Figure 1. Relative positions of LISPB stations, LUST line and KEQ epicentre in Scotland. Abbreviations are: MT, Moine Thrust; SF, Strathconan Fault; GGF, Great Glen Fault; LTF, Loch Tay Fault; HBF, Highland Boundary Fault; SUF, Southern Uplands Fault;

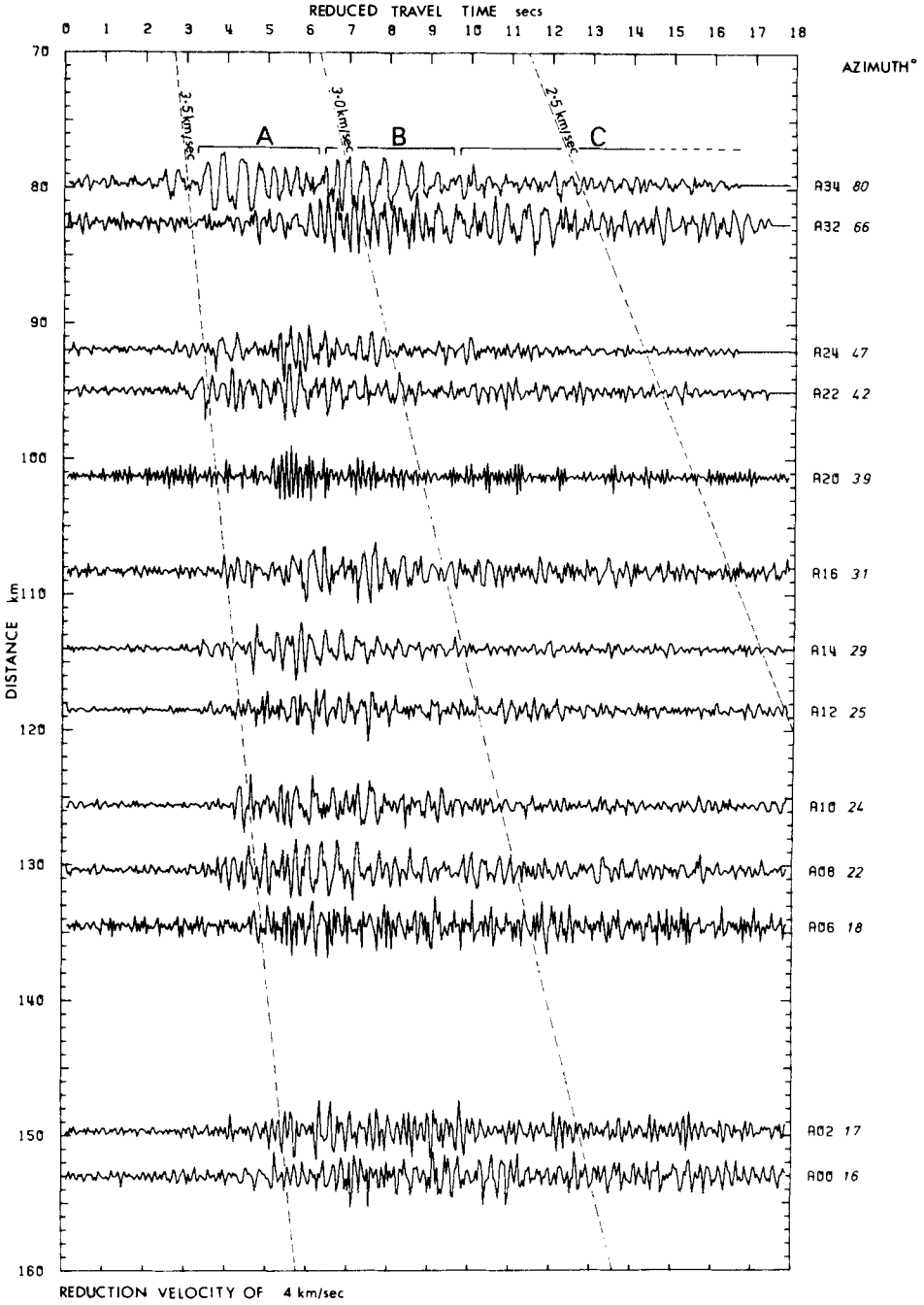

Figure 2. Vertical component recordings of KEQ along the first section of the ALPHA line.

A, second higher mode.
B, first higher mode.
C, unidentified arrival/s.

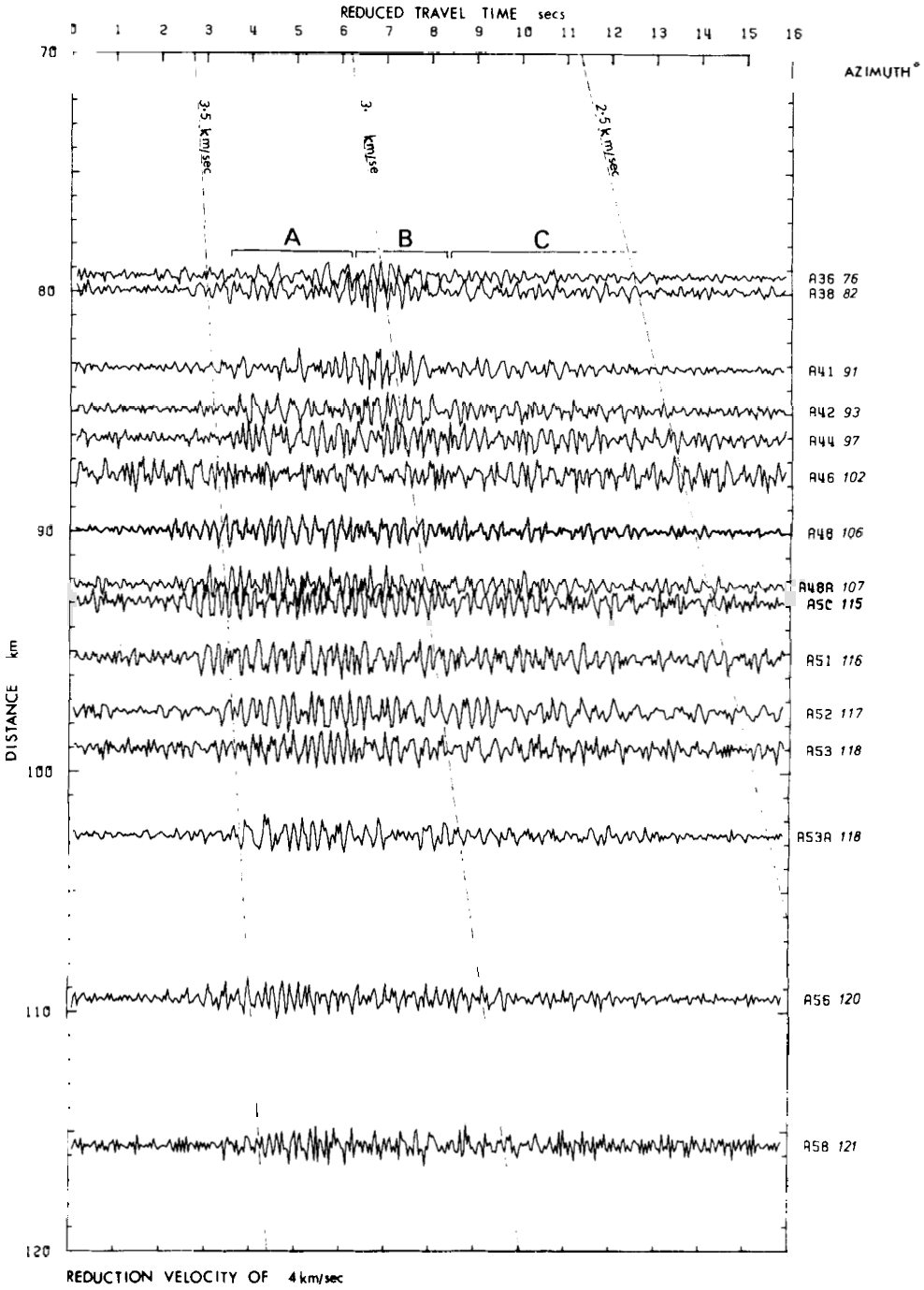

Figure 3. Vertical component recordings of KEQ along the remaining segment of the ALPHA line. Arrivals as in Fig. 2.

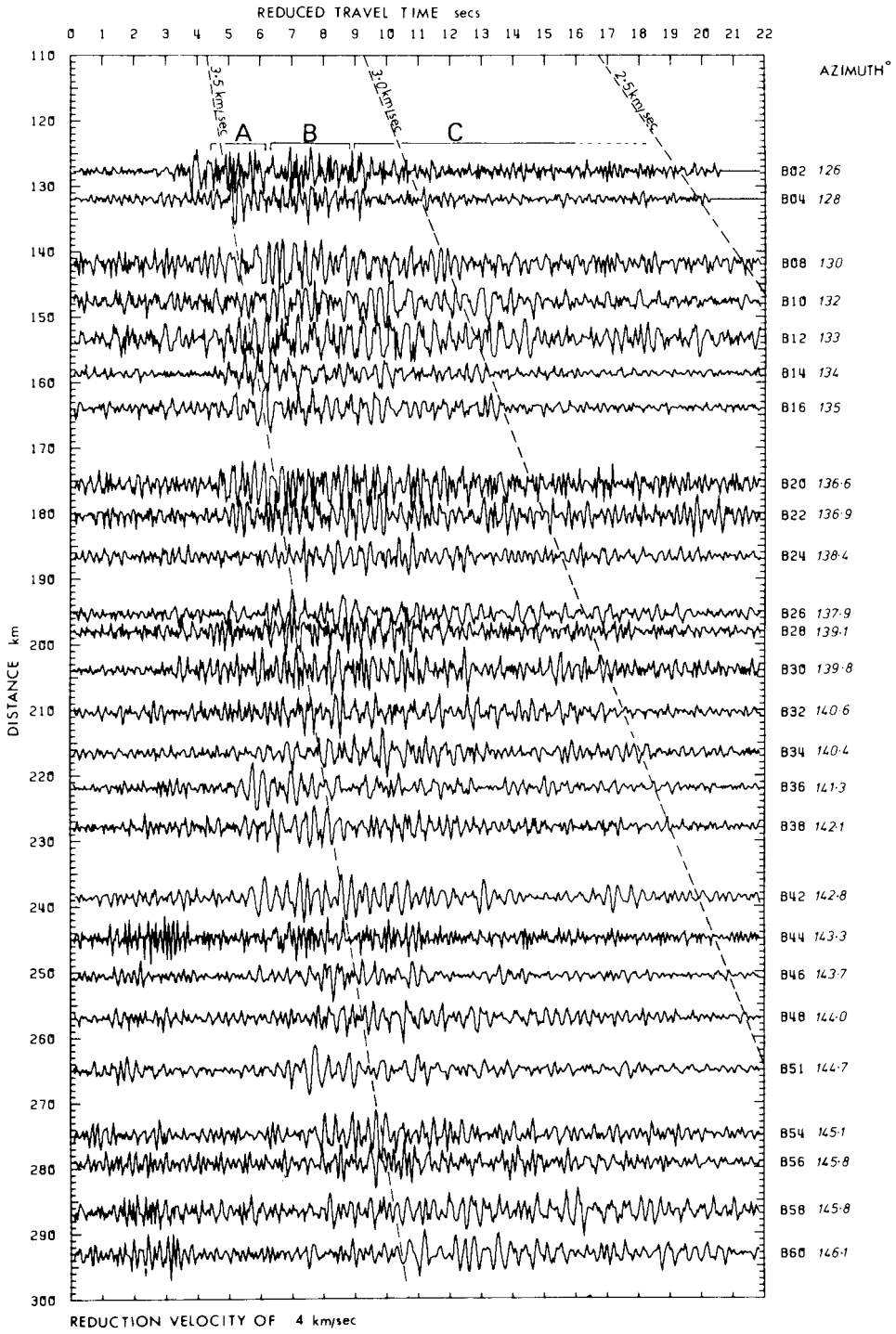

Figure 4. Vertical component recordings of KEQ along the BETA line. Arrivals as in Fig. 2.

the latter portion of the surface wave train is uncertain – it could be coda from the other two arrivals.

The surface waves generated by KEQ and recorded on the LISPB short-period instruments have energy up to 4.8 Hz, with a dominant frequency of about 2 Hz. On average, the second higher mode arrives at 3.5 km s^{-1} and the first higher mode at 3.1 km s^{-1}. The smaller amplitude waves arrive with a velocity of 2.9 km s^{-1} or less. The fluctuations in arrival time along the ALPHA line decrease towards the BETA line mainly as a result of the propagation paths covering a narrower azimuthal range. The data for the BETA line are generally of a poorer quality than those for the ALPHA line and have a much smaller signal to noise ratio. However, the separation between the first and second higher modes, and the interfering *S*-wave and second higher mode is greater for this line, thus helping to isolate the individual signals.

2.2 DISPERSION ANALYSIS

The selected higher mode waveforms are baselined, cosine-tapered, and zeros added to increase the array number to a power of 2. Spectra are then obtained using the fast Fourier transform algorithm of Cooley & Tukey (1965), the seismogram then being corrected in the frequency domain for the effects of the seismometer. The size of the time series array is chosen to accommodate different seismogram lengths and is maintained constant for the complete data set. This ensures that each set of group velocities are evaluated at the same Fourier harmonics. For the data used here the separation between adjacent harmonics is 0.024 Hz. Group velocities are derived from the seismogram using Burton & Blamey's (1972) modification of the multiple filter technique of Dziewonski, Bloch & Landisman (1969). This is adapted for high-frequency work by changing the filter constants and altering the procedure for searching the ridge of Rayleigh-wave energy to take account of *S*-wave interference. This procedure displays the Rayleigh waves on a contour diagram in the group velocity–frequency domain. The group velocity of each mode can be found by following the separate ridges representing the different modes across the diagram.

A typical contour diagram of instantaneous amplitudes in the group velocity–frequency plane is shown for the recording at station A34 in Fig. 5. The higher modes are well separated along the velocity axis but the main energy peaks have a similar frequency content. As the lower frequencies of the first higher mode interfere with the second higher mode, automatic following of the ridge crest is inhibited. Consequently, the group velocities are obtained by visual inspection of the contour diagrams. In some cases the mode energy overlaps making discrimination difficult. Each mode is selected on the basis of a simple time window around the seismogram. Shear waves interfere mainly with the second higher mode but are clearly separated on the contour diagrams for the majority of seismograms due to their higher frequency content and smaller dispersion (see shaded region of Fig. 5).

The data are averaged every four frequency harmonics to produce smooth curves, the separation between the spectral estimates now being 0.096 Hz. To increase the precision and reliability of each group velocity observation, and for the purposes of computing a standard deviation on each datum, adjacent group velocities showing similar dispersion characteristics are averaged. These standard deviations are one order of magnitude larger than the errors arising from inaccurate travel times, epicentral distances and instrument corrections, which are therefore not considered. Group velocity corrections due to the initial phase of the source (Knopoff & Schwab 1968) are of second-order importance for KEQ, as the phase is a weak function of frequency. Seven sets of group velocities are obtained, the regions covered being labelled A–G (Fig. 6). Table 1 lists the LISPB stations corresponding to each group. The regions represent relatively homogeneous provinces with respect to wave velocity.

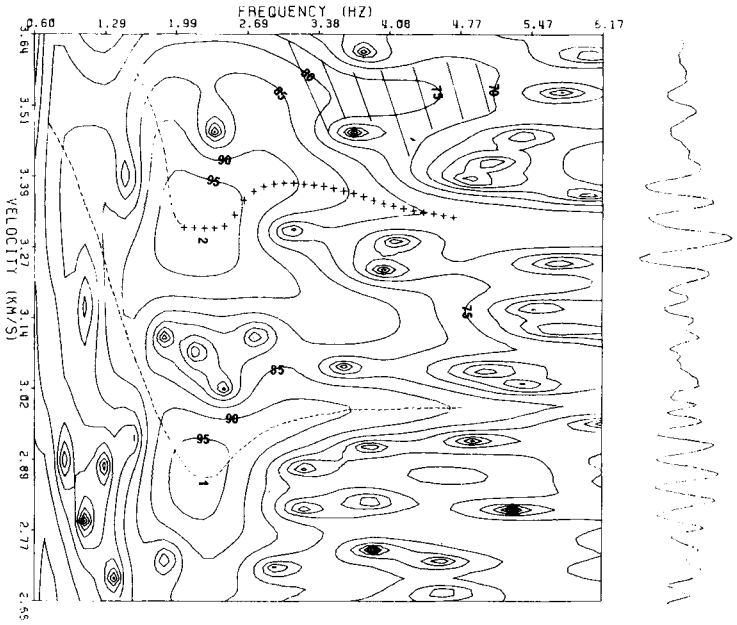

Figure 5. Contour diagram of first (1) and second (2) higher modes for station A34; shaded region corresponds to possible shear-wave energy.

- - - group velocity inferred from contours.
+ + + group velocity picked automatically by the analysis algorithm.

The smoothed sample averages of group velocities and standard deviations are shown in Figs 7 and 8. The second higher mode group velocity curve lies above the first higher mode curve in all cases, implying that there are no low-velocity zones at depth. The frequency range for the higher of the two modes is 1.8–4.8 Hz, while it is 0.8–4.8 Hz for the lower one. The standard deviations for the second higher modes are generally smaller, which could indicate a more homogeneous earth structure at greater depth in the crust. The number of stations contributing to each group varies along the line. As the group velocities are very similar along the BETA line, group G contains 25 stations. Group D, on the other hand, covers a large azimuthal range with three stations.

As the surface geology is an expression of the lithology in the upper few kilometres of the crust, we expect it to influence only the high-frequency group velocity. To examine this effect, the curves are compared with a sketch map of the surface geology of Scotland (Fig. 6). The propagation paths corresponding to groups A–E pass through the high-velocity Moine province which dominates most of northern Scotland. Groups F and G contain paths which pass through the slower Carboniferous and Old Red Sandstone rocks of the Midland Valley. The high-frequency group velocities in Figs 7 and 8 do not correlate with these observations. Instead, there is a noticeable decrease in the high-frequency group velocity at groups C, D and E, with the lowest value at group D. This is particularly clear for the first higher mode, which is presumably more sensitive to the surface structure. Groups B and F have similar dispersion characteristics and group G has the largest high-frequency velocities, this again being more noticeable for the first higher mode. Figs 7 and 8 imply a $0.4\,\mathrm{km\,s^{-1}}$ lateral variation in group velocity across Scotland.

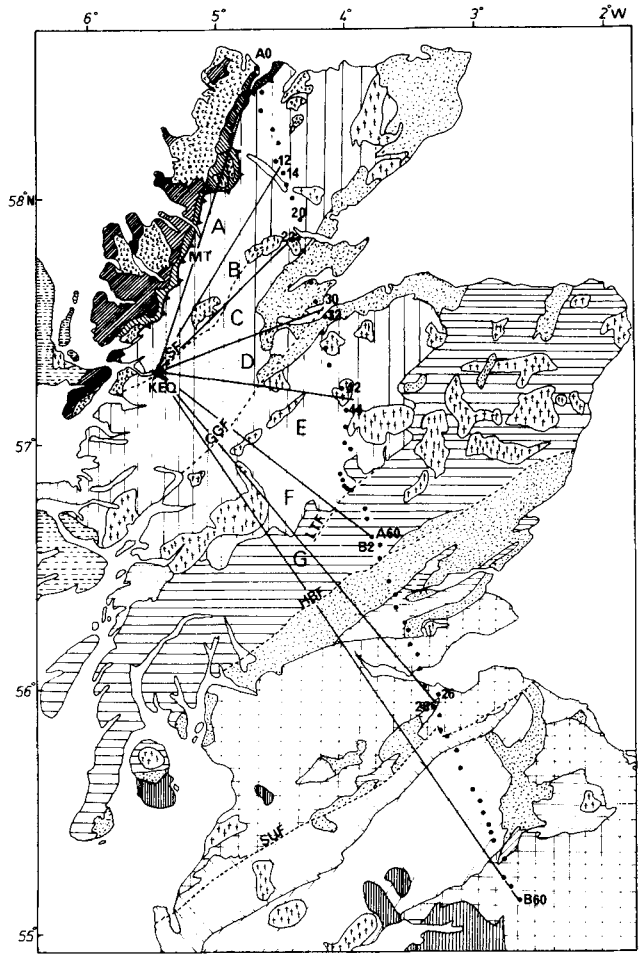

Figure 6. Regionalization of Scotland based on the group velocity dispersion characteristics of first and second higher Rayleigh modes generated by the earthquake KEQ in relation to sketch map of surface geology in Scotland. Abbreviations as for Fig. 1.

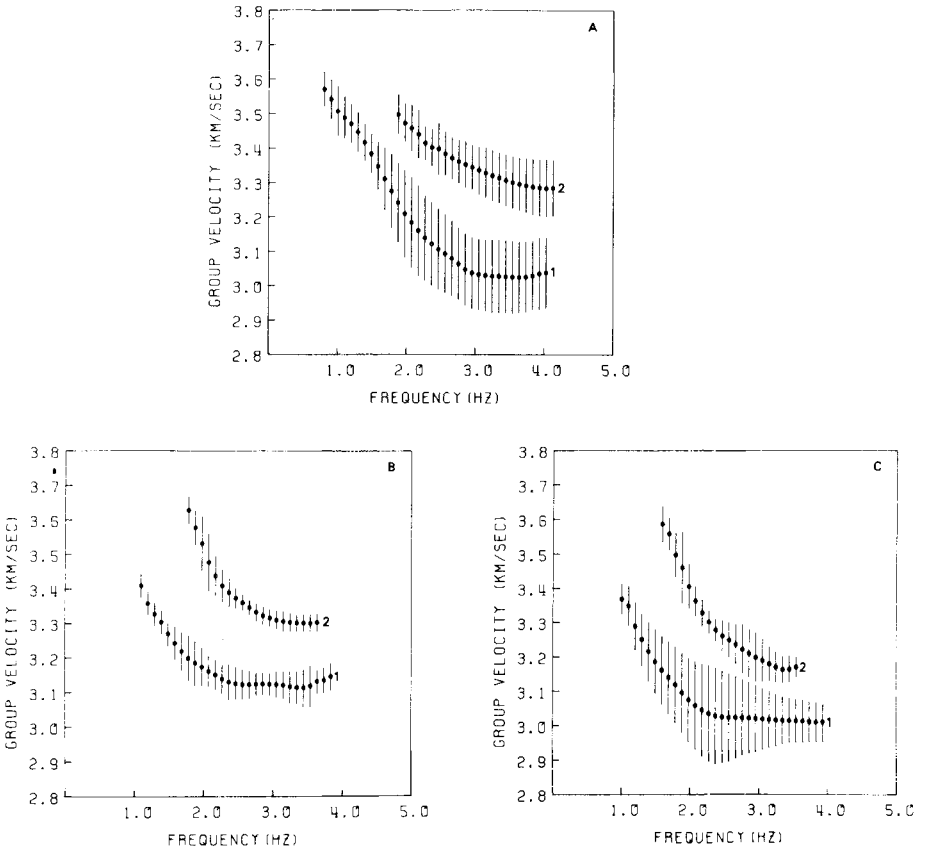

Figure 7. Smoothed averages of first (1) and second (2) higher mode group velocities with corresponding standard deviations for regions A, B and C.

2.3 CHECK ON MODE IDENTIFICATION

As the focal depth of KEQ is much larger than the expected wavelength of fundamental mode surface waves (0.5–4 km), higher mode energy is preferentially excited within the frequency range of the seismometers. A similar phenomenon has been observed for deep earthquakes (Okal 1979). Higher modes, however, have a number of critical depths at which they are excited most efficiently and frequencies at which they are not excited at all (Forsyth 1976). Only modes with non-zero depth-eigenfunctions at the earthquake focus will be excited. It is therefore necessary to check that the original qualitative identifications in the seismogram are correct. For this purpose, theoretical group velocity dispersion curves for fundamental, first and second higher modes are computed using the shallow northern and southern Moine province models of Evans (1981) (obtained by inverting fundamental mode Rayleigh-wave data), combined with the Bamford *et al.* (1978) LISPB values (converted to shear velocity) for depths between 2 and 20 km. These are superimposed upon the averaged curves for both modes from all groups in Fig. 9. The fundamental mode velocities clearly do not come close to any of the observations, a significant change in the Evans (1981) data being required for a match. Although the gradients of the theoretical higher mode curves are not as smooth as those of the observations there is a good correspondence,

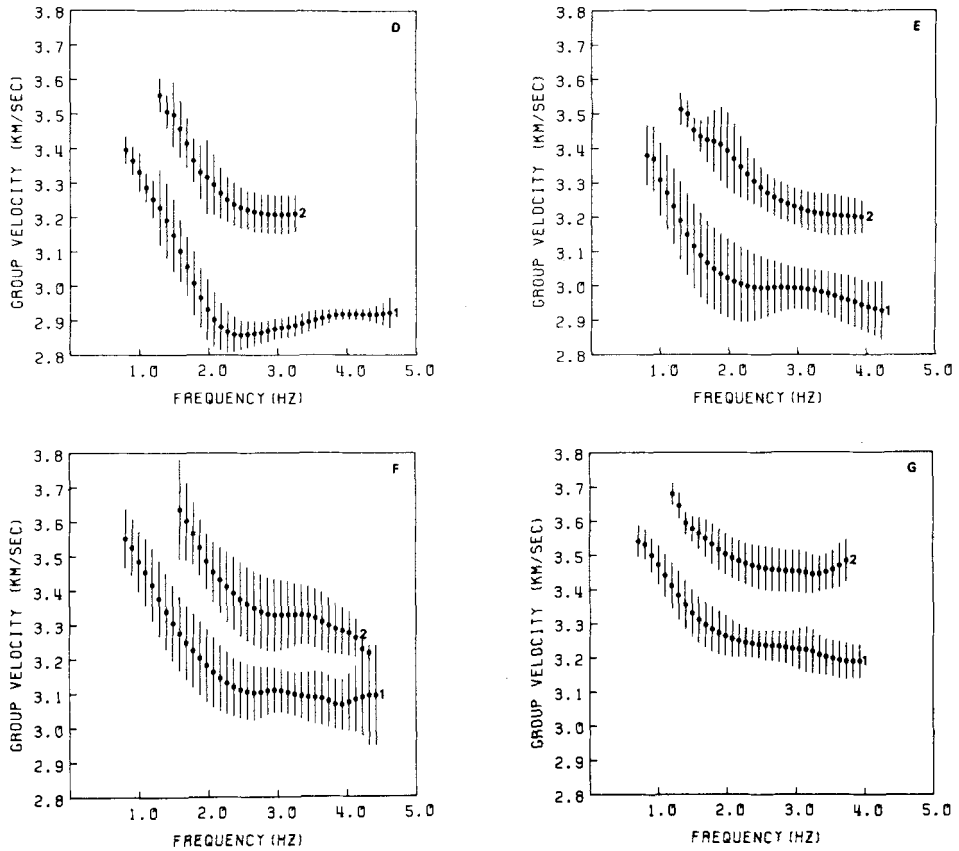

Figure 8. Smoothed averages of first (1) and second (2) higher mode group velocities with corresponding standard deviations for regions D, E, F and G.

the theoretical second higher mode curves lying slightly above the observations. These correspondences identify the observed second arrival as the first higher mode and the first arrival as the second higher mode. The theoretical dispersion curves for the third higher mode lie above those for the second higher mode and are therefore not considered in the analysis. On the basis of this identification we now invert the observed dispersion curves.

3 Inversion procedure

To facilitate the inversion of the higher mode group velocity curves, we approximate the distribution of the elastic constants in the earth by a finite number of flat homogeneous layers, overlying a half-space. The number of parameters specifying this structure is further reduced by utilizing the relationship between compressional wave velocity α and shear wave velocity β

$$\alpha = \left(\frac{2(1-\sigma)}{1-2\sigma}\right)^{\frac{1}{2}} \beta, \tag{1}$$

where σ is Poisson's constant. The depth distribution of σ is taken from Assumpção & Bamford (1978). A connection is also made between density ρ and β via the empirical

Table 1. Grouping of stations along the LISPB line which yield dispersion curves with similar characteristics.

	VELOCITY DISPERSION GROUPINGS	
	FIRST HIGHER MODE	SECOND HIGHER MODE
A	A00, A02, A06, A08, A10, A12	A00, A02, A06, A08, A10, A12
B	A14, A16, A20	A14, A16, A20
C	A22, A24	A22, A24, A30
D	A32, A34, A36, A38, A41, A42	A32, A34, A36, A38, A41, A42
E	A44, A48, A50, A51, A52, A53	A53A, A56, A58
	A53A, A56, A58	
F	B02, B04, B08, B10, B12, B14	B02, B04, B08, B10, B12, B14
	B16, B20, B22, B24, B26	B16, B20, B22, B24, B26
G	B28, B30, B32, B34, B36, B38	B28, B30, B32, B34, B36, B38
	B42, B44, B46, B48, B51, B54	B42, B44, B46, B48, B51, B54
	B56, B58, B60	B56, B58, B60.

relation used by Stuart (1978)

$$\rho = 0.286\,\beta + 1.736. \tag{2}$$

This reduction of the independent model variables is justified as the Rayleigh waves are in general more sensitive to changes in the shear constants than other structural parameters (Bloch *et al.* 1969). Each layer is now specified by β and a layer thickness. The corresponding group velocities for this model can be readily computed using (1), (2) and the theory of Schwab & Knopoff (1970). In our inversion scheme, the layer thicknesses are fixed and β in each layer is estimated from the higher mode dispersion data.

Although group velocity may occasionally be a highly non-linear function of shear velocity (Cloetingh, Nolet & Wortel 1980), small perturbations in the shear velocity of an initial earth model can be connected to corresponding fluctuations in the higher mode group velocities at different frequencies by an approximately linear relation:

$$\begin{bmatrix} \delta U_1^1 \\ \vdots \\ \delta U_l^1 \\ \delta U_1^2 \\ \vdots \\ \delta U_m^2 \end{bmatrix} = \begin{bmatrix} \frac{\partial U_1^1}{\partial \beta_1} & \cdots & \frac{\partial U_1^1}{\partial \beta_n} \\ \vdots & & \vdots \\ \frac{\partial U_l^1}{\partial \beta_1} & \cdots & \frac{\partial U_l^1}{\partial \beta_n} \\ \frac{\partial U_1^2}{\partial \beta_1} & \cdots & \frac{\partial U_1^2}{\partial \beta_n} \\ \vdots & & \vdots \\ \frac{\partial U_m^2}{\partial \beta_1} & \cdots & \frac{\partial U_m^2}{\partial \beta_n} \end{bmatrix} \begin{bmatrix} \delta\beta_1 \\ \vdots \\ \delta\beta_n \end{bmatrix}. \tag{3}$$

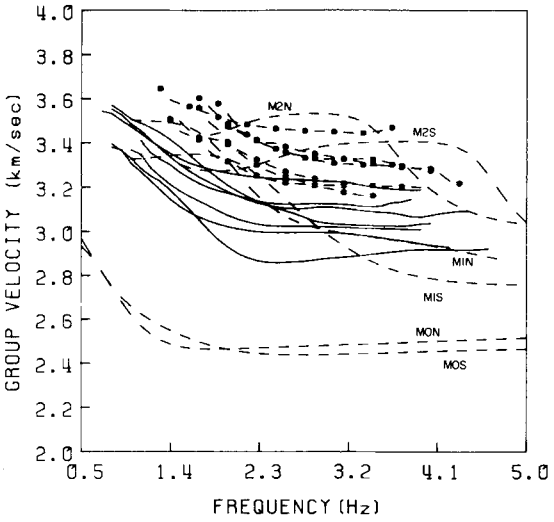

Figure 9. Comparison of observed first and second higher mode group velocities for the regions A–G (see Fig. 6) with theoretical fundamental, first and second higher mode dispersion derived from the near surface Moine models of Evans (1981) and data of Bamford *et al.* (1978).

M0N, fundamental mode
M1N, first higher mode
M2N, second higher mode
} northern Moine Province.

M0S, fundamental mode
M1S, first higher mode
M2S, second higher mode
} southern Moine Province.

———— first higher modes from groups A to G.
–●–●–●– second higher modes from groups A to G.

l and m are the number of data points in the first and second higher mode curves respectively, n is the number of layers in the model, δU_j^i is the difference between the group velocity datum corresponding to a trial model and the observed group velocity for the ith mode and jth frequency, $\partial U_j^i/\partial \beta_k$ is the first term in a Taylor's series expansion of group velocity about the dispersion for an initial trial model, and $\delta \beta_k$ is the parameter change, which is to be determined, in the kth layer of the model.

The group velocity derivatives are calculated numerically by first-order differences. Examination of these in the matrix of (3) provides a physical insight into the inversion problem. They display the dependence of the theoretical curves on the model at particular frequencies and can be used to compare the different information contributed by the two higher modes. Fig. 10(b,c) displays the derivatives as a function of frequency for each layer in the model. The shapes of the curves for each mode are similar. This implies an overlap of the information contributed by the two modes. Consequently, simultaneous inversion of the group velocities should result in a more reliable and accurate determination of the common structural parameters and be an improvement on those from independent inversions. Corresponding plots of the partial derivatives with respect to α and ρ (keeping other parameters constant) are shown in Fig. 11, demonstrating the relative insensitivity of the group velocity to these parameters.

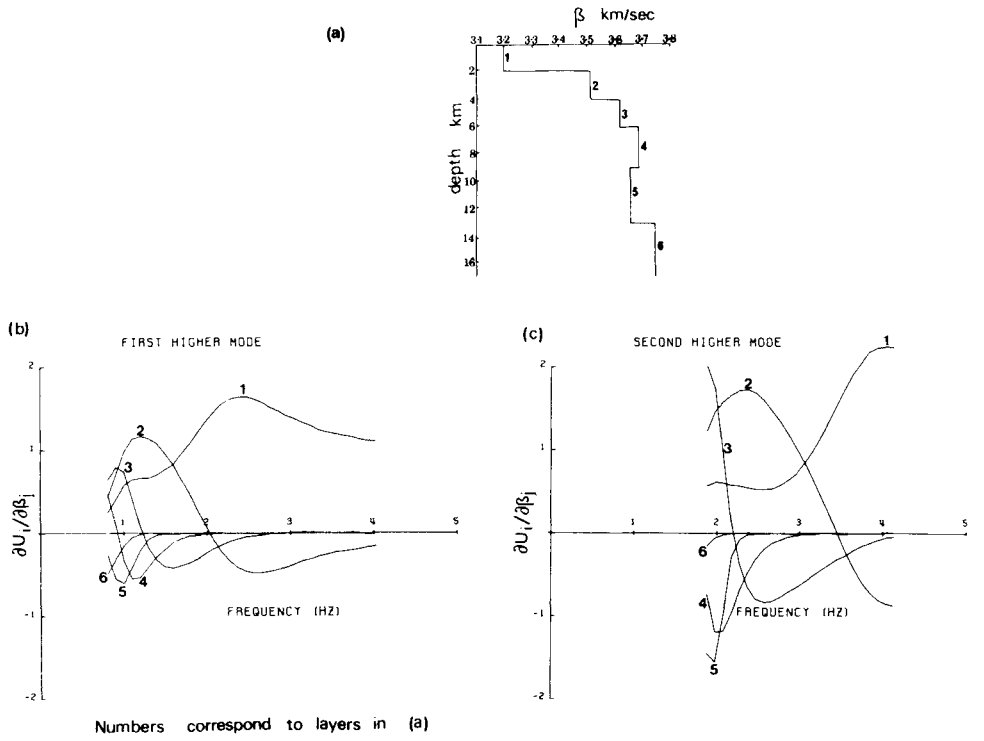

Figure 10. Higher mode partial derivatives of group velocity with respect to shear velocity ($\partial U_j^i/\partial \beta_k$) for a typical LISPB/KEQ shear velocity model shown in (a), as a function of frequency (b) and (c). Numbers correspond to layers in velocity model of (a).

The general inverse problem in (3) is solved using the Lanczos (1961) inverse matrix stabilized by introducing the Levenberg–Marquardt parameter θ (Lawson & Hanson 1974), this giving an estimate of the model parameter corrections required to reduce the difference between theoretical and observed curves. To take account of the varying uncertainty between data points and the differing thicknesses between layers in the model, the solutions are calculated using vectors and matrices weighted according to the standard errors on the observations and the inverse of model layer thicknesses (Wiggins 1972), the half-space being weighted equally with the layer above it. For non-zero θ, the solution estimates cease to be independent. The Lanczos (1961) inverse yields a quantitative evaluation of the extent of this effect via the resolution matrix, resolving kernels corresponding to the matrix rows (Der, Massé & Landisman 1970). Uncertainties on the estimated parameters for this particular inverse are also obtained as a function of θ (Crosson 1976). Here, θ affects a trade-off between these two quantities (Jackson 1972). As (3) is only a first approximation, it is applied many times in an iterative process. Initially, θ is set large enough to give a stable solution and is then varied at each iteration until the function

$$\chi_v^2 = \frac{1}{l+m-n-1}\left[\sum_{i=1}^{l}\left(\frac{\delta U_i^1}{\Delta U_i^1}\right)^2 + \sum_{i=1}^{m}\left(\frac{\delta U_i^2}{\Delta U_i^2}\right)^2\right]$$

reduces below a threshold value. ΔU_j^i is the standard deviation on the datum corresponding to the ith mode and jth frequency. This formula is used to express the fit at a particular level

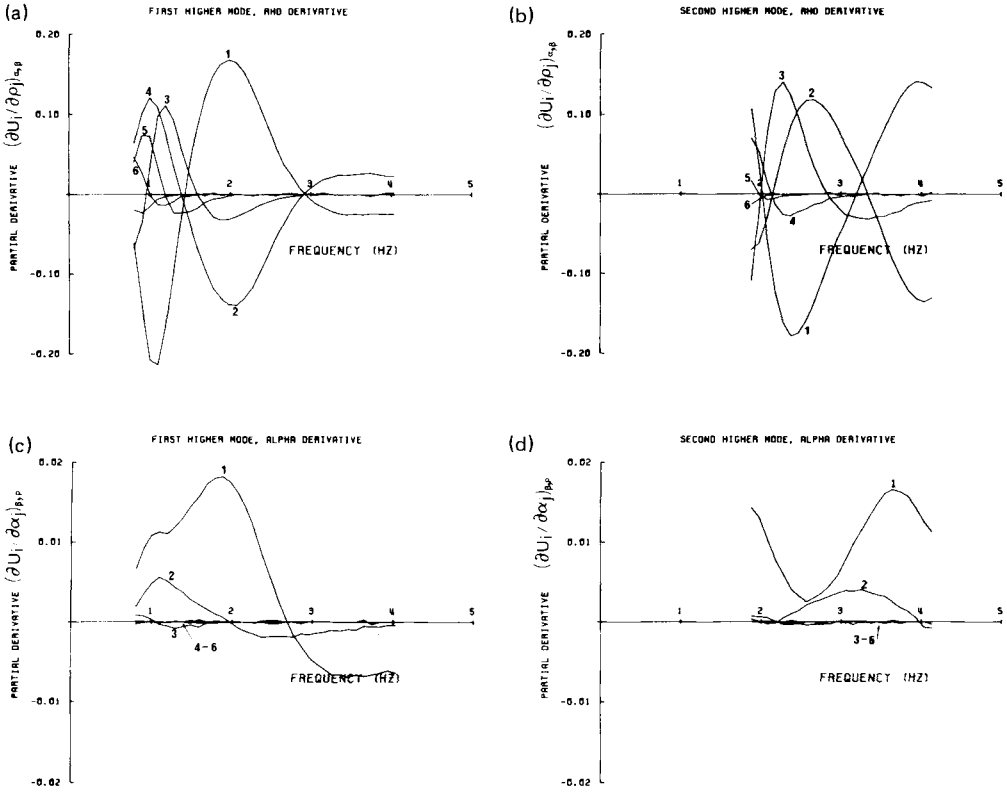

Figure 11. Higher mode partial derivatives of group velocity with respect to density $(\partial U_j^i/\partial \rho_k)_{\alpha,\beta}$ (a and b) and compressional wave velocity $(\partial U_j^i/\partial \alpha_k)_{\beta,\rho}$ (c and d), corresponding to the typical LISPB/KEQ model shown in Fig. 10(a), as a function of frequency.

of significance corresponding to the number of degrees of freedom in the system (Bevington 1969).

4 Shear velocity results from inversions and discussion

The bandwidth for higher mode propagation through the structure is limited by the low- and high-frequency cut-offs. These are determined by the depth to the model half-space and the thickness of the top layer of the model respectively. The low-frequency limit is satisfied by the trial and error of different velocity models. Instabilities, which govern the choice of the minimum layer thickness, oppose the high-frequency cut-off effect, which is therefore set at 2 km for these data. The thickness of successively deeper layers is increased with depth to compensate for the expected decrease of resolution with depth. This reduces unwanted negative side-lobes in the resolution kernels and provides a more definitive interpretation of the results. Each group velocity region is given the same layering, with thicknesses of 2, 2, 2, 3 and 4 km overlying a half-space. The choice of initial velocity models for the inversion uses the results of Evans (1981) and Bamford *et al.* (1978) as a guide.

An attempt is made to invert the combined data sets to a 1 per cent significance level, only group B fails to meet this requirement, being fitted to a 10 per cent level. The results of a typical inversion are shown in Fig. 12. The diagram compares the observations and

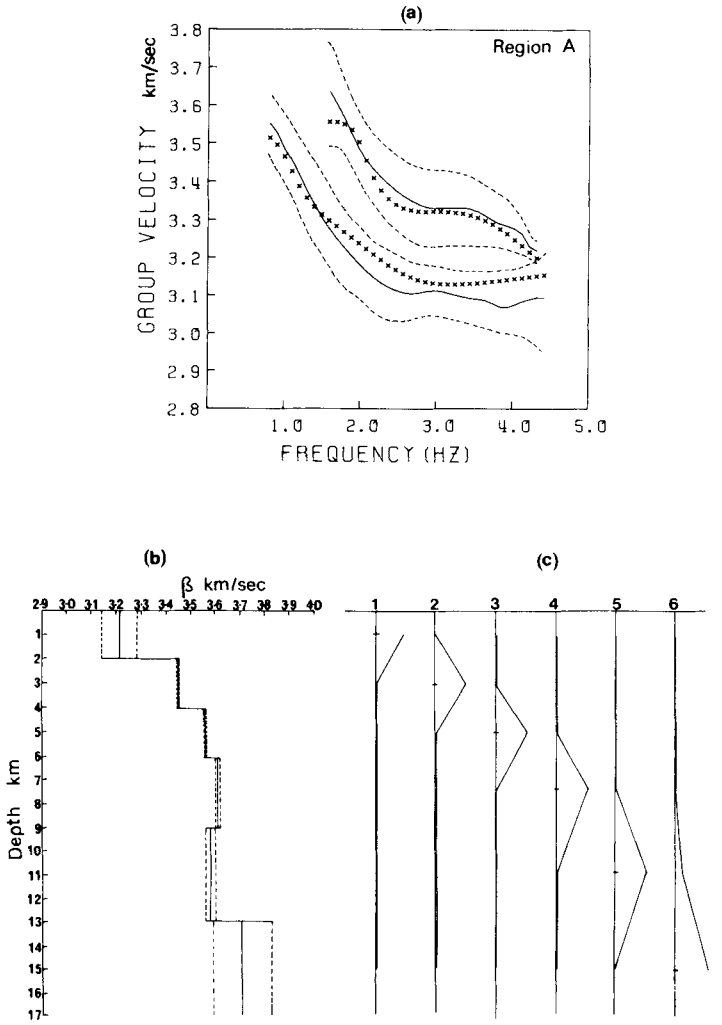

Figure 12. Simultaneous inversion results for group velocity dispersion data from first and second higher mode Rayleigh waves in region A. (a) Comparison between theoretical higher mode group velocity points generated by the shear velocity model found by the inversion (xxx) and observed curves (—). Dotted lines indicate standard deviations on the observations. (b) Shear velocity model with bounds obtained by simultaneous inversion of observed first and second higher mode group velocities and standard deviations. (c) Resolution kernels associated with the inversion. Kernels are normalized with respect to their individual maximum and horizontal ticks mark the centre of the corresponding layer.

standard deviations with the final theoretical curves. It also presents the errors on the model parameters and resolution kernels associated with the standard deviations on the observations and the chosen value of β. All the estimated shear velocity profiles are plotted in Fig. 13 together with a profile obtained by averaging each layer velocity.

In the majority of inversions the high-frequency theoretical group velocity for the second mode is an underestimate of the observed dispersion, and the velocity for the first higher mode is an overestimate. A possible cause of this could be *S*-wave interference with the higher modal frequencies. β in each model increases with depth, there being a distinctive

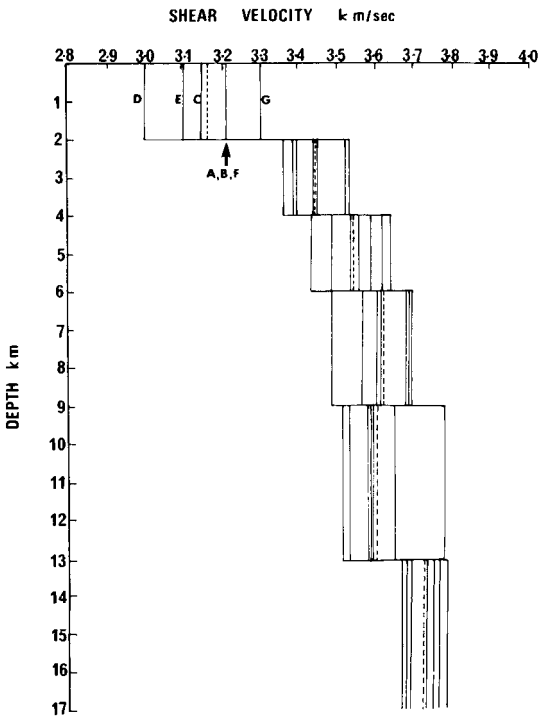

Figure 13. Summary of shear velocity–depth profiles for regions A–G obtained by simultaneous inversion of first and second higher mode group velocity data. The dotted lines indicate the average velocity in each layer taken over all regions. As the profiles group closely, only the top layer velocities are marked for the different regions.

jump between the top layer (with a mean velocity of 3.15 km s^{-1}) and the lower layers (with a mean velocity of 3.60 km s^{-1}). The standard deviations on the model velocities generally increase with depth, although for several models the smallest uncertainty occurs in a layer other than the deepest. This is due to the particular energy distribution of the higher modes.

Fig. 13 clearly shows that all of the profiles are consistent with this apparently low-velocity upper 2 km of the crust. In interpreting this it must be noted that the layer velocity represents an average over 2 km, and so the low-velocity effect could quite possibly be confined to the upper few 100 m. A low-velocity surficial layer could be caused by cracks or a weathered layer. The shear velocity gradient is a consistent 3.4–3.8 km s^{-1} increase within a depth range 2–17 km in the upper crust. There is a slight decrease in β between 9 and 13 km depth, followed by a 0.15 km s^{-1} increase in velocity. The shear velocities for the bottom layer are closely grouped. This general increase with depth could be explained by the increasing lithostatic overburden pressure on the rocks. The variation of β in the top layers does not correlate with any surface geological expression, the low velocities of the Midland Valley do not affect the models for regions F and G (Fig. 6). This reinforces the conclusions of Section 2.2. The slowest structure corresponds to group D and the fastest to those of group G or B.

To compare our results with the available refraction data the shear velocity models are converted to compressional wave models using the Assumpção & Bamford (1978) distribution of σ. The fastest and slowest velocity profiles (corresponding to groups D and G

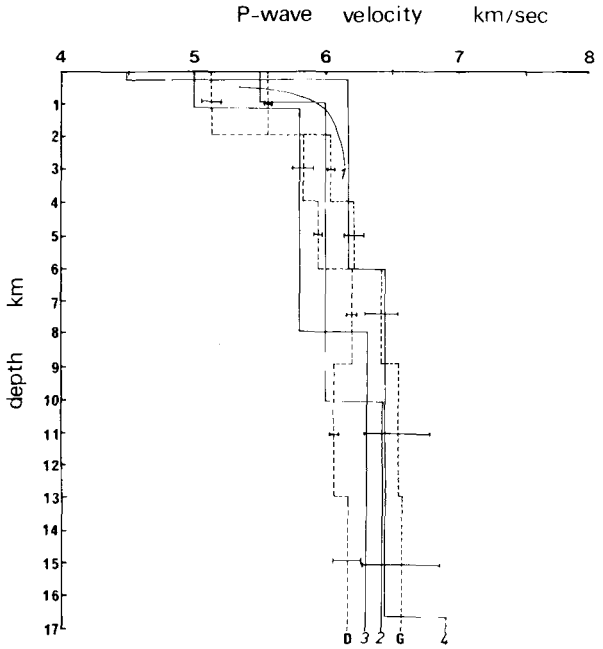

Figure 14. Comparison of compressional wave velocity profiles for Scotland inferred from shear-wave models obtained by simultaneous inversion of higher modes and Assumpção & Bamford's (1978) Poisson's ratio distribution, with those calculated from refraction experiments in similar regions.

D, group D which has the lowest velocities.
G, group G which has the fastest velocities.
1, mean velocity–depth curve derived from LUST velocity distribution (Hall 1978).
2, preliminary velocity–depth distribution extracted from Kaminski *et al.* (1976).
3, LISPB profile south of BETA line
4, LISPB profile north of ALPHA line
} Bamford *et al.* (1978).

respectively) are plotted in Fig. 14 together with the uncertainties in each layer velocity. The mean velocity distribution for the LUST line of Hall (1978), which was north-west of the LISPB lines (Fig. 1) is also shown in Fig. 14. Profiles at the northern tip of the ALPHA line and southern tip of the BETA line are extracted from the three layered crustal model of Bamford *et al.* (1978). Finally, the preliminary velocity distribution used by Kaminski *et al.* (1976) to obtain a KEQ epicentral solution is compared. Fig. 15 compares columns of the average compressional wave velocities as a function of crustal depth for regions A–G and the northern LISPB results.

All the profiles in Fig. 14 are in good agreement, particularly below 10 km where the refraction experiment models are within the uncertainty bounds on the velocity structure for group G. Fig. 15 shows that the averaged inversion results are only 0.2 km s^{-1} different from those of the northern LISPB profile between 4 and 16.5 km depth. The model for group D lies closer to the southern LISPB structure and the group G (similar to group B) model is closer to the northern structure. The largest difference between velocity distributions occurs, as expected, in the upper few kilometres of the crust since this region is most sensitive to surface inhomogeneities. The northern LISPB model, in particular, has a 4.3 km s^{-1} surficial layer compared to an average velocity of 5.4 km s^{-1} in a 2 km thick layer for the surface wave results. If the fundamental mode was discernible in the data this

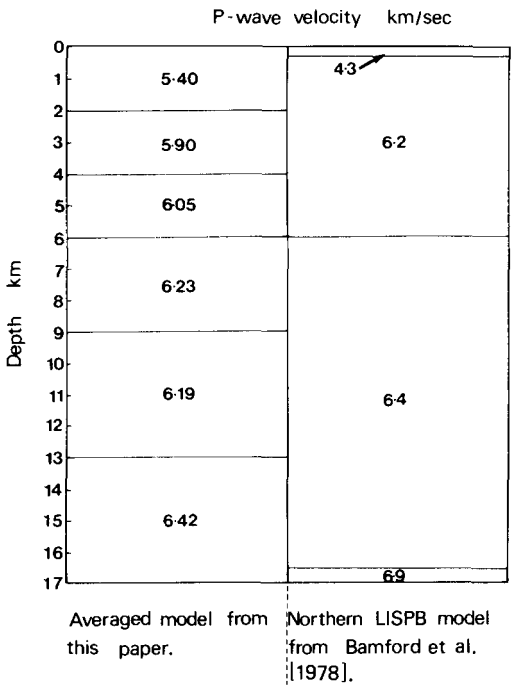

Figure 15. Schematic representation of average compressional velocities as a function of depth for results in this paper and LISPB profile north of ALPHA line (Bamford *et al.* 1978) corresponding to the curve shown in Fig. 14.

surface feature could have been better resolved. As the velocities obtained using the surface waves represent an average over the paths from epicentre to recording stations, these cannot readily be used in interpreting the north-westerly trend of decreasing depth to the Lewisian granulites (Bamford *et al.* 1978).

5 Conclusions

Higher mode Rayleigh-wave data generated by the earthquake KEQ were recorded on the short-period seismometers of the LISPB array. The two prominent Rayleigh waves were identified quantitatively by matching the group velocity dispersion curves with theoretical data computed using prior information for the area. It appears that only the first and second higher mode waves were recorded within the instrument pass-band. The area of Scotland covered by the paths from this event may be divided into seven apparently homogeneous regions on the basis of similar group velocity characteristics. The regionalization yields an estimate of the extent of the lateral variations in shear velocity with depth along western Scotland by a simultaneous inversion of the higher mode group velocities in each sector. The profiles are well resolved down to depths of 17 km and show a clear jump of 0.3 km s^{-1} between the 2 km thick top layer and the lower layers. This discontinuity does not necessarily indicate a transition at 2 km depth, but represents a smoothed discontinuity between these layers. There is a slight gradient between 2 and 17 km depth, β increasing from about 3.4 to 3.8 km s^{-1}. The shear velocity in the top layer of the models varies regionally by 0.4 km s^{-1}, but does not correlate with the surface geological expression for the area of Scotland covered in the analysis.

The simultaneous inversion of first and second higher mode data has yielded well resolved shear-wave velocity-depth models which complement the compressional-wave velocity models obtained from refraction studies and elucidates structures at comparable depths.

Acknowledgments

This work was completed as part of a PhD project at the British Geological Survey, Edinburgh and the University of Edinburgh. We are grateful to Bob McGonigle and Graham Neilson for useful discussions at various stages of this work. It was supported by the Natural Environment Research Council, to whom CDM is grateful for a studentship, and is published with the approval of the Director of the British Geological Survey (NERC).

References

Assumpção, M., 1981. The NW Scotland earthquake swarm of 1974, *Geophys. J. R. astr. Soc.*, **67**, 577–586.

Assumpção, M & Bamford, D., 1978. LISPB V – Studies of crustal shear waves, *Geophys. J. R. astr. Soc.*, **54**, 61–73.

Bamford, D., Faber, S., Jacob, B., Kaminski, W., Nunn, K., Prodehl, C., Fuchs, K., King, R. & Willmore, P., 1976. A lithospheric seismic profile in Britain – I. Preliminary results, *Geophys. J. R. astr. Soc.*, **44**, 145–160.

Bamford, D., Nunn, K., Prodehl, C. & Jacob, B., 1977. LISPB III – Upper crustal structure of northern Britain, *J. geol. Soc. London*, **133**, 481–488.

Bamford, D., Nunn, K., Prodehl, C. & Jacob, B., 1978. LISPB IV – Crustal structure of northern Britain, *Geophys. J. R. astr. Soc.*, **54**, 43–60.

Bevington P. R., 1969. *Data Reduction and Error Analysis for the Physical Sciences*, McGraw-Hill, New York.

Bloch, S., Hales, A. L. & Landisman, M., 1969. Velocities in the crust and upper mantle of southern Africa from multi-mode surface wave dispersion, *Bull. seism. Soc. Am.*, **59**, 1599–1629.

Braille, L. W. & Keller, G. R., 1975. Fine structure of the crust inferred from linear inversion of Rayleigh wave dispersion, *Bull. seism. Soc. Am.*, **65**, 71–83.

Burton, P. W. & Blamey, C., 1972. A computer program to determine the spectrum and dispersion characteristics of a transient seismic signal, *AWRE Rep. No. 0/48/72*, HMSO, London.

Cloetingh, S. A. P. L., Nolet, G. & Wortel, M. J. R., 1980. Standard graphs and tables for the interpretation of Rayleigh wave group velocities in crustal studies, *Proc. K. ned. Akad. Wet., B*, **83**, 101–118.

Cooley, J. W. & Tukey, J. W., 1965. An algorithm for the machine calculation of complex Fourier series, *Maths Comput.*, **19**, 297–301.

Crosson, R. S., 1976. Crustal structure modeling of earthquake data – 1. Simultaneous least squares estimation of hypocenter and velocity parameters, *J. geophys. Res.*, **81**, 3036–3046.

Der, Z., Massé, R. & Landisman, M., 1970. Effects of observational errors on the resolution of surface waves at intermediate distances, *J. geophys. Res.*, **75**, 3399–3409.

Dziewonski, A. M., Bloch, S. & Landisman, M., 1969. A technique for the analysis of transient seismic signals, *Bull. seism. Soc. Am.*, **59**, 427–444.

Dziewonski, A. M. & Hales, A. L., 1972. Numerical analysis of dispersed seismic waves, in *Methods in Computational Physics*, **11**, 39–85, Academic Press, New York.

Evans, A. C., 1981. Propagation and dissipation of VHF Rayleigh waves in Scotland, *PhD thesis*, University of Edinburgh.

Forsyth, D. W., 1976. Higher mode Rayleigh waves as an aid to seismic discrimination, *Bull. seism. Soc. Am.*, **66**, 827–841.

Hall, J., 1978. 'LUST' – a seismic refraction survey of the Lewisian basement complex in NW Scotland, *J. geol. Soc. London*, **135**, 555–563.

Jackson, D. D., 1972. Interpretation of inaccurate, insufficient and inconsistent data, *Geophys. J. R. astr. Soc.*, **28**, 97–109.

Kaminski, W., Bamford, D., Faber, S., Jacob, B., Nunn, K. & Prodehl, C., 1976. A lithospheric seismic profile in Britain – II. Preliminary report on the recording of a local earthquake, *J. Geophys.*, **42**, 103–110.

Knopoff, L. & Schwab, F. A., 1968. Apparent initial phase of a source of Rayleigh waves, *J. geophys. Res.*, **73**, 755–760.

Knopoff, L. & Schlue, J. W., 1972. Rayleigh wave phase velocities for the path Addis Ababa – Nairobi, *Tectonophys*, **15**, 157–163.

Lanczos, C., 1961. *Linear Differential Operators*, Van Nostrand, London.

Lawson, C. L. & Hanson, R. J., 1974. *Solving Least Squares Problems*, Prentice-Hall, Englewood Cliffs.

Nolet, G., 1975. Higher Rayleigh modes in western Europe, *Geophys. Res. Lett.*, **2**, 60–62.

Nolet, G., 1977, The upper mantle under western Europe inferred from the dispersion of Rayleigh modes, *J. Geophys.*, **43**, 265–285.

Okal, E. A., 1979. Higher-mode Rayleigh waves studied as individual seismic phases, *Earth planet. Sci. Lett.*, **43**, 162–167.

Schwab, F. A. & Knopoff, L., 1970. Surface wave dispersion computations, *Bull. seism. Soc. Am.*, **60**, 321–344.

Stuart, G. W., 1978. The upper mantle structure of the North Sea region from Rayleigh wave dispersion, *Geophys. J. R. astr. Soc.*, **52**, 367–382.

Wiggins, R. A., 1972. The general linear inverse problem: implications of surface wave and free oscillations for earth structure, *Rev. Geophys. Space Phys.*, **10**, 251–285.